NUMERICAL MODELING OF DELAMINATION IN GFRP COMPOSITES[1)]

M. R. K o s h r a v a n, A. Y o u r d k h a n i

Faculty of Engineering
Mechanical Engineering Department
University of Tabriz, Tabriz, Iran

Polymer matrix composites have become highly relevant structural materials. However, high performance laminates are quite susceptible to transverse cracking and delamination. Transverse cracks may cause significant stiffness losses, accelerate environmentally induced degradation and generate delamination. The characterization and modeling of fracture behavior is thus highly relevant for the design of composite parts. In this paper, the delamination phenomena in the Mixed Mode I+II which is one of the important cause of failure in multilayer composites, are studied. The composite is a GFRP (Glass Fiber Reinforced Plastic) and are studied under static monotonic loading. Using the Irwin–Kies criteria, usual laws of elasticity and VCCT (Virtual Crack Closure Technique), based on finite element method, the SERR (Strain Energy Release Rate) in Mode I, Mode II, and four ratio Modes (G_I/G_{II}) are evaluated. The finite element analysis of test bars is carried out using ANSYS5.5 software in two dimensions, and the appropriate boundary conditions are chosen. Our numerical results are compared with known experimental ones and with application of the local effects, such as three-dimensional (3D) effect in the width of the test bar with the shape of MMB (Mixed Mode Bending) specimen, scattering between experimental and numerical results is evaluated and discussed. For the 3D effect, the variation of the stress components in the mid-plane of specimen in which delamination occurs, versus the width of specimen, is obtained. Then the variation of strain energy release rate in different ratio Modes, in the width of test bars is calculated.

1. INTRODUCTION

Composite laminates are one of the most useful materials for the engineering structures, because of their high strength ratio to their weight. A glass-fiber epoxy resin composite is one of those composites that its application, because of its high resistance in tension, the low commercial price of its fibers compared to others, such as carbon fibers, and its resistance against corrosion, has increased [1]. When a multilayer composite is loaded, the interlaminar stresses appear in the interface of the layers. Theses stresses lead to delamination [2], which is one of the most important mechanisms of rupture of the composite materials (Fig. 1) [3].

[1)]GFRP – Glass Fiber Reinforced Plastic.

Hence prediction of delamination and also fracture toughness of these materials is useful to their amelioration. In the present research the Uni-Directional (UD) GFRP were modeled. The modeling of a multilayer composite with different orientation of fibers in each layer will be done in the future researches. In this case, the evaluation of interlaminar stresses before modeling of delamination is important [4].
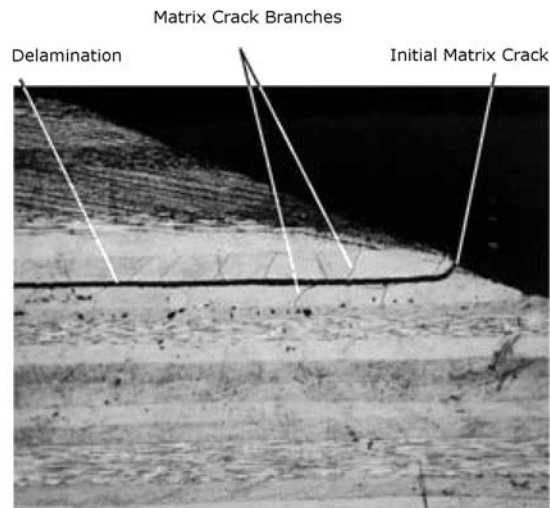

Fig. 1. Delamination in a composite material.

In the mechanism of delamination which is analogous to the crack growth in isotropic materials, all the possibilities of rupture shown in Fig. 2 exist [5]. Testing of Mode I is standardized by ISO using DCB (Double Cantilever Beam) specimen and several researches carried on Mode II using ENF (End Notched Flexure) [6] and ELS (End Loaded Split) specimen are well advanced. In reality delamination doesn't occur in a pure mode. Hence investigation on the Mixed Mode seems to be important [7].
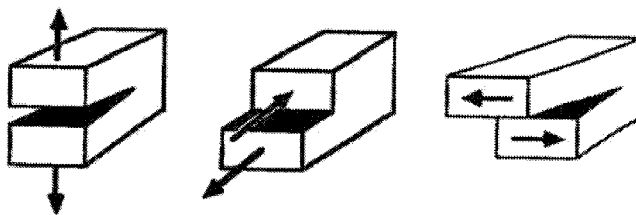

Fig. 2. Modes of rupture.

2. MMB SPECIMEN

Different tests of delamination on the Mixed Mode I + II such as CTS (Compact Tension Specimen) and CLS (Crack Lap Shear) are presented [8]. The most useful specimen for the Mixed Mode is the MMB specimen. Crews and Reeder, with the composition of DCB and ENF specimens, have presented a MMB specimen [9]. The first concept of MMB test device, in order to decrease the linear geometrical errors, which reached about 30%, was redesigned in order to eliminate the moment of the loads around the pins through which it is applied to the specimen [10]. In the corrected concept, the nonlinear errors are decreased to less than 3% and finally the test device is designed as shown in Fig. 3 [11].
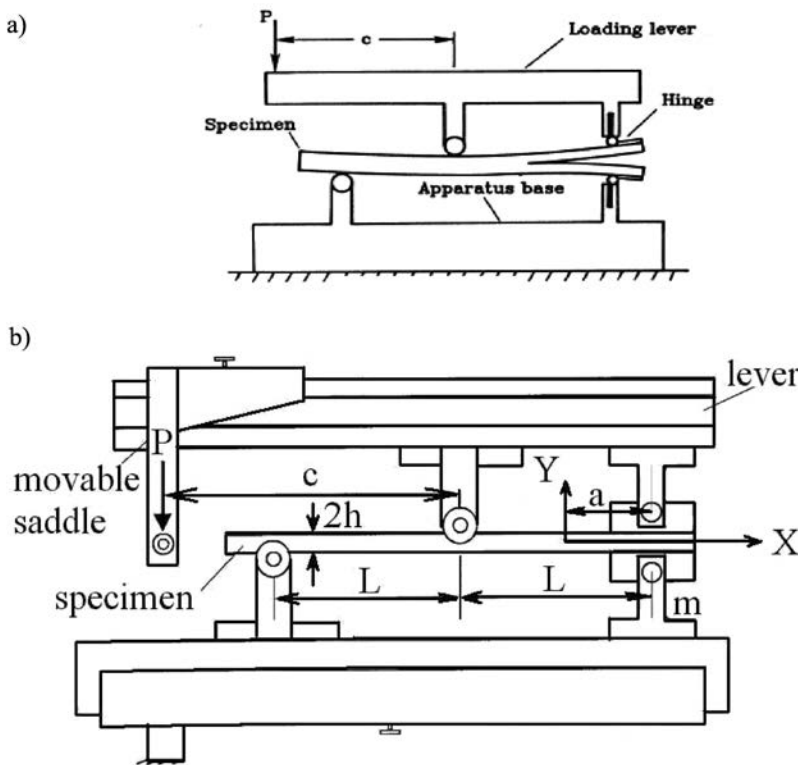

FIG. 3. MMB test apparatus [10]: a) schematic form; b) test apparatus with the device.

The manner of Mode I and Mode II loading composition and their application to the specimen are shown in Fig. 4 [9]. We can apply the forces using the unique load P through a lever, having I shape. If this load reaches its critical value, delamination will occur. The length of the lever c determines the ratio of the loads and then the ratio of the Modes. When the load P is applied in

the middle of the span of the beam, $(c = 0)$, the test bar will be loaded in the pure Mode II, and with increasing c, the ratio G_{II}/G_T (G_T is the total SERR) decreases. By moving the lever and lifting it on the hinge, the pure Mode I loading occurs. Dimensions and mechanical properties of the uni-directional glass fiber epoxy resin composite, which is used in our numerical analysis, are given in the Table 1 [11].
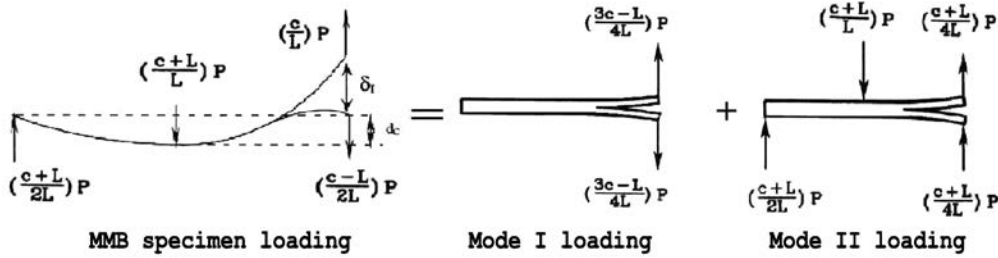

FIG. 4. MMB specimen loading.

Table 1. Mechanical properties and geometry of the test bar.

Specimen Dimension	Mechanical Property	
$L = 65$ mm	$E_{11} = 25.7$GPa	$(\pm 8\%)$
$2h = 5$ mm	$E_{22} = 6.5$ GPa	$(\pm 8\%)$
$b = 20$ mm	$G_{12} = 2.5$ GPa	$(\pm 8\%)$
$L_T = 150$ mm	$\upsilon_{12} = 0.32$	$(\pm 8\%)$
$a_0 = 35$ mm	$\nu_{\text{fiber}} = 35.4\%$	$(\pm 8\%)$
	$\nu_{\text{void}} = 4.2\%$	$(\pm 8\%)$

3. THEORY OF STRAIN ENERGY RELEASE RATE

In this theory, the Irwin–Kies relationship is given as follows [12]:

$$(3.1) \qquad G = \frac{P^2}{2b} \frac{\partial C}{\partial a},$$

$$(3.2) \qquad C = \delta/P.$$

In this relationship P is the applied load, b is the width of specimen, C is the compliance, a is the crack length and δ is the deflection in the point of the load application. When G reaches its critical value (G_{IC}), delamination initiates.

4. Beam theory

Using the elementary theory of beams and their substitution in the relations of Irwin–Kies, we can obtain the relations for the strain energy release rate. According to Fig. 4, the Mode I and Mode II components of loading are given as follow [10]:

$$
P_{\mathrm{I}} = \left(\frac{3c - L}{4L}\right) P,
$$

(4.1)

$$
P_{\mathrm{II}} = \left(\frac{c + L}{L}\right) P.
$$

Using the elementary beam theory for the DCB and the ENF specimens, the Mode I and Mode II components of the SERR are obtained [10]:

$$
G_{\mathrm{I}} = \frac{12a^2 P_{\mathrm{I}}^2}{b^2 h^3 E_{11}},
$$

(4.2)

$$
G_{\mathrm{II}} = \frac{9a^2 P_{\mathrm{II}}^2}{16 b^2 h^3 E_{11}}.
$$

With substitution of relations (4.1) with the Eqs. (4.2), we will have:

$$
G_{\mathrm{I}} = \frac{3a^2 P^2}{4 b^2 h^3 L^2 E_{11}}(3c - L)^2,
$$

(4.3)

$$
G_{\mathrm{II}} = \frac{9a^2 P^2}{16 b^2 h^3 L^2 E_{11}}(c + L)^2.
$$

So the ratio of modes is defined as follows:

(4.4)
$$
\frac{G_{\mathrm{I}}}{G_{\mathrm{II}}} = \frac{4}{3}\left[\frac{3c - L}{c + L}\right], \qquad c \geq \left(\frac{L}{3}\right).
$$

So relation (4.4) will not be valid for the values of C less than 21.67 mm. The ratio of modes is independent of the crack length a, and depends only on the length c. Using the correction coefficients for the shape deformation corresponding to the rotation of the section of specimen at the end of the crack and also the shape of shear deformation, relation (4.3) is corrected as follows [13]:

$$
G_{\mathrm{I}} = \frac{3a^2 P^2}{4 b^2 h^3 L^2 E_{11}}(3c - L)^2\left[1 + \frac{2}{a\lambda} + \frac{1}{a^2\lambda^2} + \frac{h^2}{10a^2}\frac{E_{11}}{G_{13}}\right],
$$

(4.5)

$$
G_{\mathrm{II}} = \frac{9a^2 P^2}{16 b^2 h^3 L^2 E_{11}}(c + L)^2\left[1 + \frac{h^2}{5a^2}\frac{E_{11}}{G_{13}}\right], \qquad \lambda = \frac{1}{h}\sqrt[4]{\frac{6E_{22}}{E_{11}}}.
$$

5. Calibration method

In this method, the compliance of specimen is calculated by measuring the critical applied load (which leads to the crack growth), the crack length and the displacement of the point of load application. This experiment is carried out for test bars with different initial crack lengths and results are demonstrated by the curve of compliance versus, the crack length. If we consider two separate compliances for Mode I and Mode II components, we will have [7]:

$$C_{\mathrm{I}} = \frac{\delta_I}{P_{\mathrm{I}}} = Ka^n,$$

(5.1)

$$C_{\mathrm{II}} = \frac{\delta_{\mathrm{II}}}{P_{\mathrm{II}}} = C_0 + ma^3.$$

In these relations P_{I} and P_{II} are determined with relation (4.2). n and m are obtained respectively from slope of the curves $Ln(C_{\mathrm{I}}) - Ln(a)$ and $C_{\mathrm{II}} - a^{1/3}$. δ_{I} is obtained directly by measurement of the opening of the crack. Displacement d_c is measured in the support, as shown in Fig. 4 and δ_{II} is calculated as follows [7]:

$$\delta_{\mathrm{II}} = \Delta + d_c m,$$

(5.2)

$$\Delta \approx \delta_{\mathrm{I}}/4.$$

Thus, Mode I and Mode II components of SERR are evaluated using the following relations [7]:

$$G_{\mathrm{I}} = \frac{n P_{\mathrm{I}} \delta_{\mathrm{I}}}{2ab},$$

(5.3)

$$G_{\mathrm{II}} = \frac{3ma^2 P_{\mathrm{II}}^2}{2b}.$$

In another method for obtaining SERR in Mode I, C is considered as a function of $(a + |\Delta|)^3$ and Δ is determined using the curve $C_{\mathrm{I}}^{1/3} - a$. As a result, the following relation is obtained. Δ indicates the phenomena of shear and rotation at the end of the crack [14].

(5.4)
$$G_{\mathrm{I}} = \frac{3 P_I \delta_I}{2b(a + |\Delta|)}.$$

6. Finite element method

In this section, VCCT method is used and the components of strain energy release rate are obtained using the following relations:

(6.1)
$$G_{\mathrm{I}} = \lim_{\Delta a \to 0} \frac{1}{2b\Delta a} p_y^0(\nu_1 - \nu_2),$$

$$G_{\mathrm{II}} = \lim_{\Delta a \to 0} \frac{1}{2b\Delta a} P_x^0(u_1 - u_2),$$

u and v are the relative displacement between nodes 1 and 2. Δa is the length of crack which should close virtually. P_x^0 and P_y^0 are the loading components, which are used for the closure of the crack (Fig. 5).
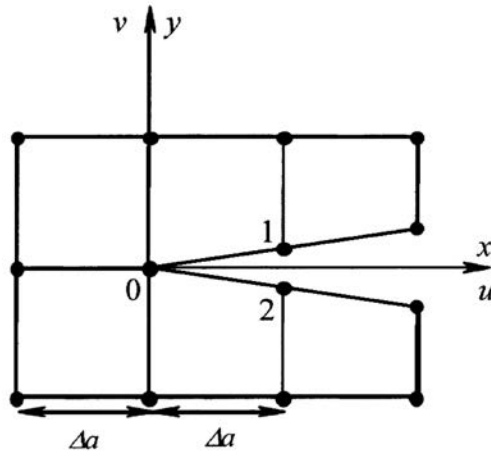
Fig. 5. The shape of elements for VCCT.

7. Finite element model of MMB specimen

For two-dimensional (2D) modeling, we have used four corners solid elements with 8 nodes and three corners solid elements with 6 nodes at crack tip. Since width of the specimen is higher than its thickness, the problem is studied in plane strain state. As the stress concentration zone is smaller than the dimensions of the specimen, the meshes are refined only in a small zone at the crack tip. We refined the meshes so that we obtained converged results. The convergence tolerance of stresses was 0.01 MPa, which was sufficiently precise for our research. Thus we don't need to include the micromechanics of the structure. The type of elements leads to singularity of the stresses and strains at the end of the crack (Fig. 6). The right and left supports of the specimen are modeled by limiting the

displacements of the nodes, but the rotation remained free. The values of the applied loads, depending on the ratio of loading mode, is calculated by relation (4.1) and applied on the nodes.
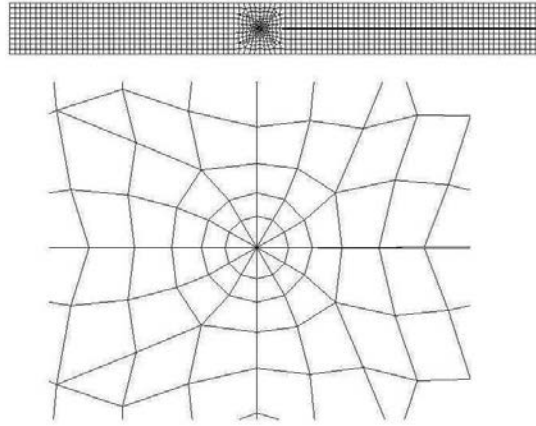

FIG. 6. Mesh generation for 2D finite element analysis.

Each test bar is in contact with two rollers and two hinges through which the load is applied (Fig. 3a). In the 2D finite element modeling, for each contact point, the boundary conditions are applied to the test bar in all of the nodes in the vicinity of the point of load application in order to take into account the contact surface of the roller and the test bar.

In three-dimensional (3D) finite element model, we have used twenty nodes solid elements. The goal of 3D modeling is analyzing the stress and strain energy along the width of specimen [15]. The elements are refined regularly at the width of the crack. The x-axis and y-axis are situated at the crack tip and z-axis is directed along of the width of specimen. As the boundary conditions and dimensions of 3D specimen are symmetrical about to the xy plane, only half of specimen is modelled (Fig. 7).
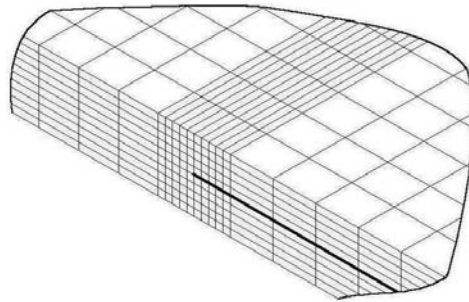

FIG. 7. Mesh generation for 3D finite element analysis.

As the Mode II of delamination is introduced in specimen, for its two cantilever parts, the lower face of the upper cantilever could slide on the upper face of the lower cantilever. So, in 2D and 3D models, contact elements are used.

8. Ruptures in the crack tip

In studying at delamination, identification of the beginning of the crack propagation is a discussible case. In this paper, with using the finite element analysis of specimen, different stresses at the end of the crack are calculated. Using rupture criteria in composite materials and stresses calculated at the crack tip, we analyze the delamination. From the mechanical point of view, fracture of the composite materials with epoxy resin matrix is similar to that occurring in the brittle materials. So the plastic zone in the crack tip is very small and in the theoretical analyses and in the finite element model, the rupture in the crack tip is considered as only elastic.

9. Experimental criterion of rupture

The point of the initiation of crack in an experimental specimen is obtained using three methods. In the first method, the crack growth leads to a deviation of the curve of load-displacement from the linear state. The point of deviation is called NL, which is not always easily distinguishable [16]. In the second method, a line with a slope smaller than 5% of the initial slope of the curve of load-displacement is considered [17]. The intersection of this line with the curve of load-displacement is the starting point of crack propagation. In the third method, point AE (Acoustic Emission), which corresponds to the registration of the first signal during the test, is defined as the beginning of the crack growth. All these criterions are shown in Fig. 8.
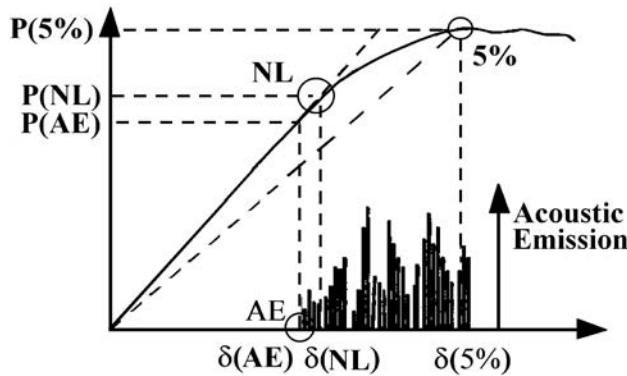

Fig. 8. Mesh generation for 3D finite element analysis.

10. Results and discussion

10.1. 2D Results

Numerical analysis of the specimen is carried out according to the experimental methods, in pure Mode I, pure Mode II, and four ratios of Mode (G_{II}/G_I) 0.25, 0.50, 0.75 and 0.89 which corresponds to the lever length c of 108.3, 56.8, 39 and 31.55mm with an initial crack length of $a_0 = 35$ mm. The stress distribution σ_x has the same shape for all of the mode ratios and it has not a significant influence on the crack growth because of high strength of the composite specimen in the x-axis direction. Figure 9 shows the σ_y stress distribution in crack zone for pure modes loading. The σ_y distribution for the mode ratios, for which Mode I exists, has the shape of two tangent circles (Bean Shape). The maximum stress in y-axis direction has the highest value and is the principal cause of crack growth in Mode I. The lowest value is in x-axis direction. Figure 10 presents the τ_{xy} distribution in crack zone for pure modes loading. The τ_{xy} distribution for the mode ratios in which Mode II exist has a spindle shape. The maximum stress in x-axis direction has the highest value and is the principal cause of crack growth

a) σ_x

b) σ_y
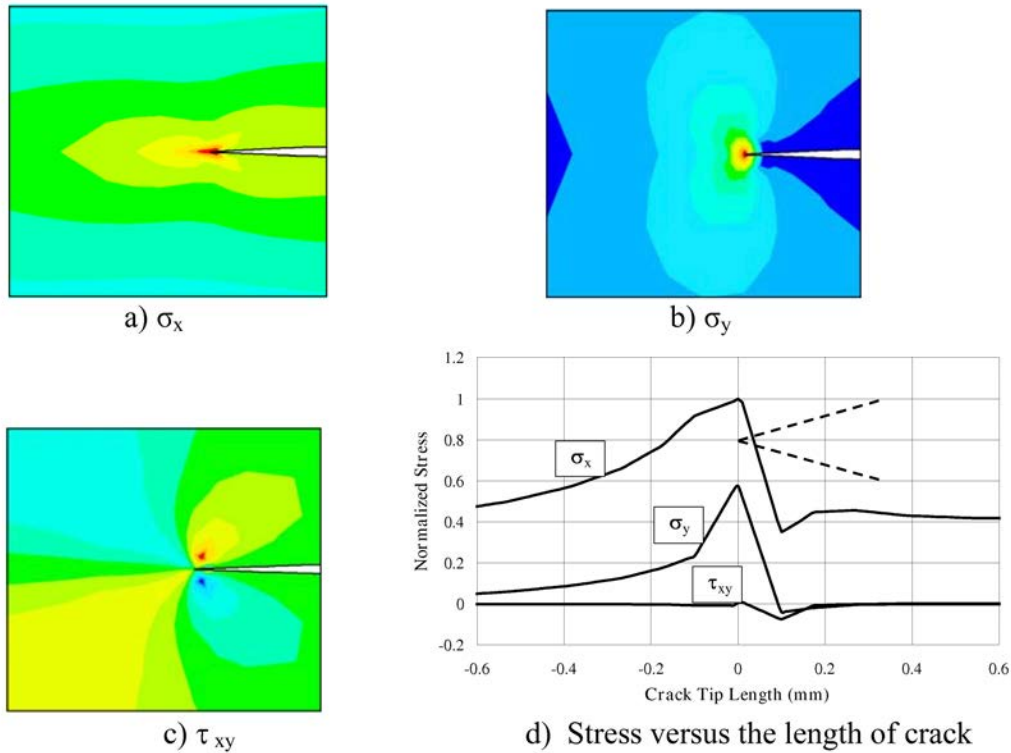
c) τ_{xy}

d) Stress versus the length of crack

Fig. 9. Stress distribution in crack zone in pure Mode I Loading of 2D model.

in Mode II. The lowest values are observed in y-axis direction. The maximum stress σ_y in pure loading of Mode II and τ_{xy} in pure loading of Mode I occurs in a zone farther than crack tip and it can deviate the crack from its principal route, (Fig. 9b and 10a).
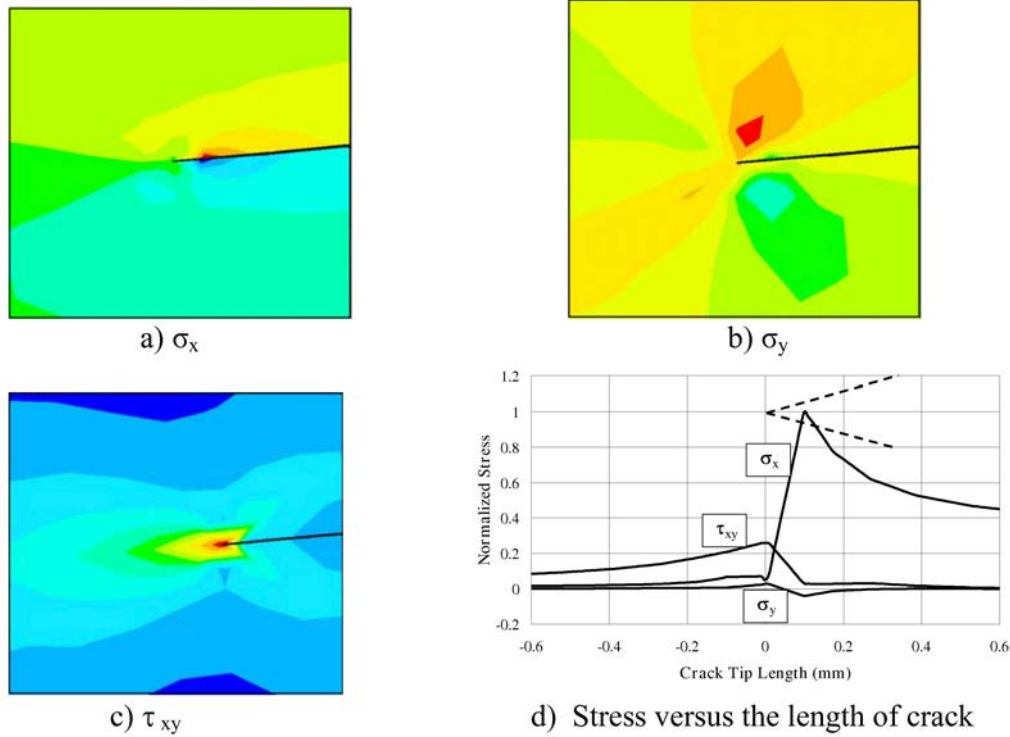

a) σ_x

b) σ_y

c) τ_{xy}

d) Stress versus the length of crack

FIG. 10. Stress distribution in crack zone in pure Mode II Loading of 2D model.

Figures 11 and 12 show Mode I and Mode II components of SERR for $G_{II}/G_T = 50\%$ versus the crack length a. The values of SERR of the beam theory G_{BT}, following relation (4.3), the corrected beam theory G_{CBT}, following relation (4.5) and calibration method G_{IC} following relation (5.3), are obtained by substituting the critical values of load and deflection obtained from numerical analysis in the corresponding relations. When the curve of load-displacement reaches its critical value, using VCCT criterion the SERR is calculated at the crack tip. As it can be observed, the strain energy release rate doesn't change too much for different crack lengths. Also the values of G_{CBT} are higher than G_{BT}. In the components of Mode I, G_{vcct} has a well corporation with calibration method, especially with relation (5.4), because the scatter doesn't exceed 1%.
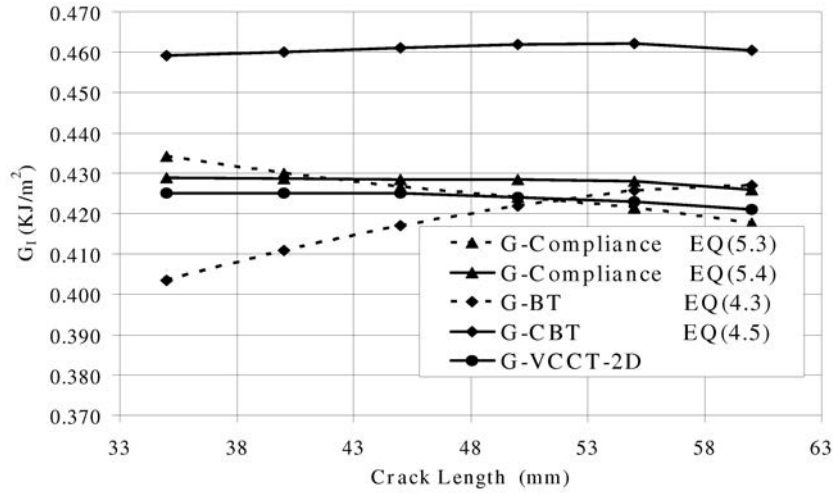
FIG. 11. The Mode I component of SERR versus crack length for the mode ratio
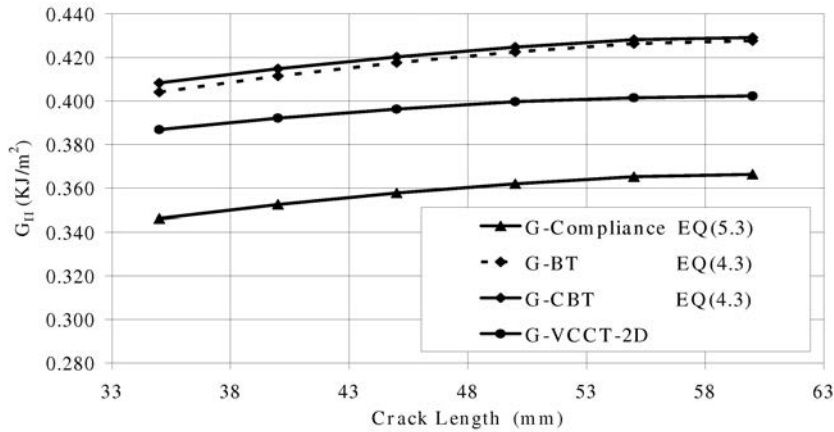$G_{\mathrm{II}}/G_T = 50\%$ in 2D model.

FIG. 12. The Mode II component of SERR versus crack length for the mode ratio
$G_{\mathrm{II}}/G_T = 50\%$ in 2D model.

10.2. 3D Results

Figures 13 to 16 present some of the stress distributions of the 3D specimen on the plane $(X\text{–}Y)$, in the vicinity of the crack. These figures explain the variation of stress in the width of specimen and 3D effects. In all of the cases, peak of the curve is situated at crack tip. The highest value of σ_x and σ_y is in the middle of specimen width and decreases in the margins, (Fig. 13 and 14). On the mode
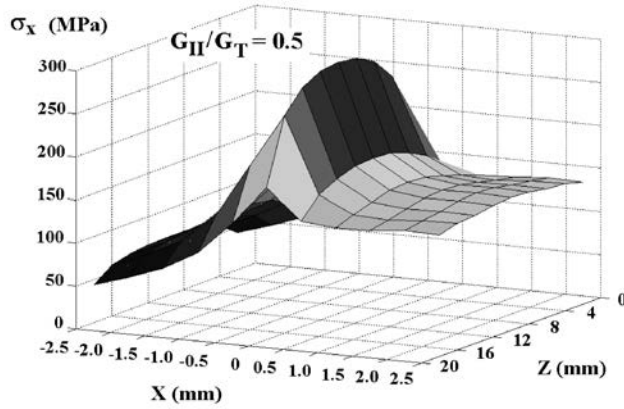
FIG. 13. σ_x distribution in the width of crack in 3D model, for the mode ratio of $G_{II}/G_T = 0.5$.
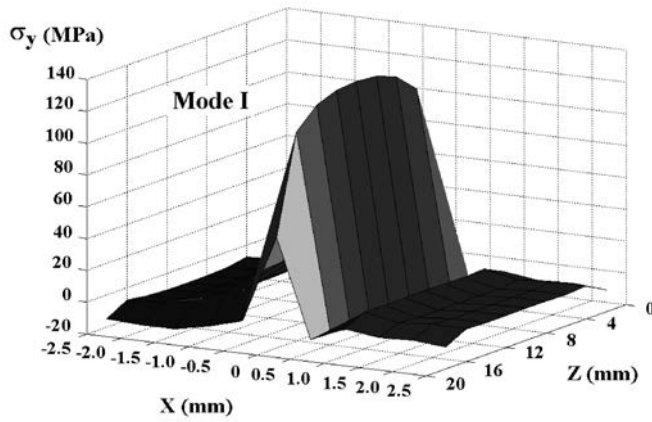

FIG. 14. τ_y distribution in the width of crack in 3D model, for pure Mode I loading.
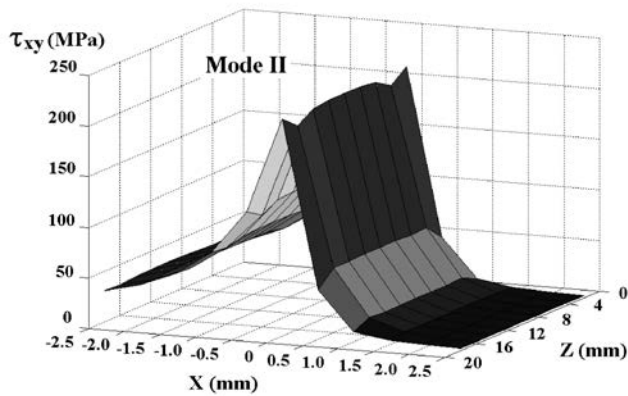

FIG. 15. τ_{xy} distribution in the width of crack in 3D model, for pure Mode II loading.
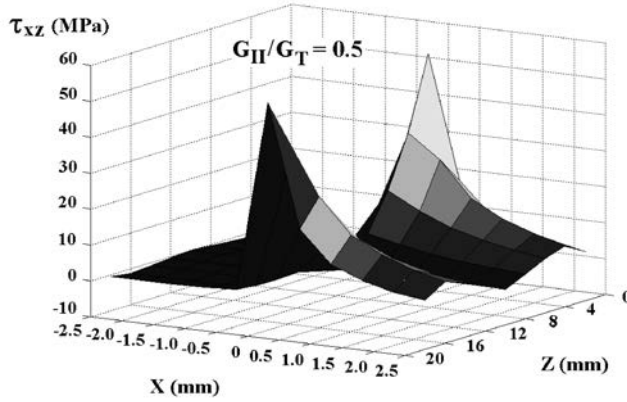
FIG. 16. τ_{xy} distribution in the width of crack in 3D model, for the mode ratio of
$G_{II}/G_T = 0.5$.

ratios which Mode II loading exists, the transversal strains of the upper and lower layers of crack plane are in opposite direction on the z-axis. This phenomenon leads to sliding of these layers on each other, maximize τ_{xz} in the margins and use a part of the strain energy for the Mode III (Fig. 16). The τ_{xy} stress distribution is a composition of the above-mentioned cases (Fig. 15).

Figure 17 shows the distribution of SERR components in the specimen width using VCCT criterion. The shape of their distribution for all ratios of modes remains as shown, with the difference that their quantity varies upon the ratio of the modes. For all ratios in which Mode II is associated, we observe a local increasing of G_{III} in the margins. The G_{total} variation in the different ratio of modes is influenced by G_I, G_{II} and G_{III} behavior (Fig. 18).
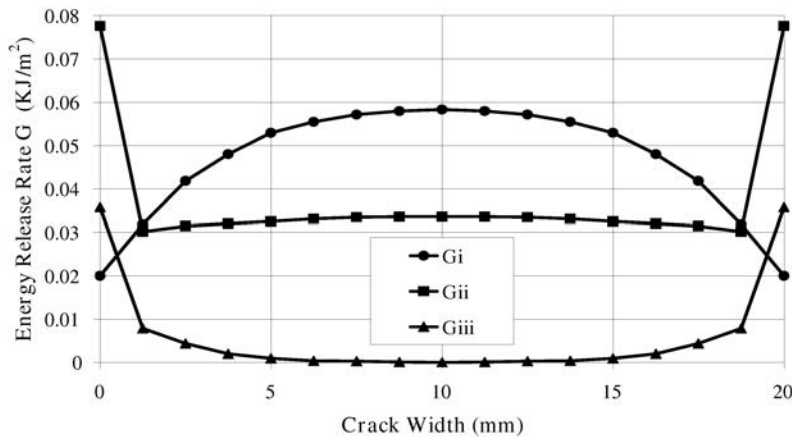

FIG. 17. Distribution of G_I, G_{II} and G_{III} in crack width with VCCT for the mode ratio
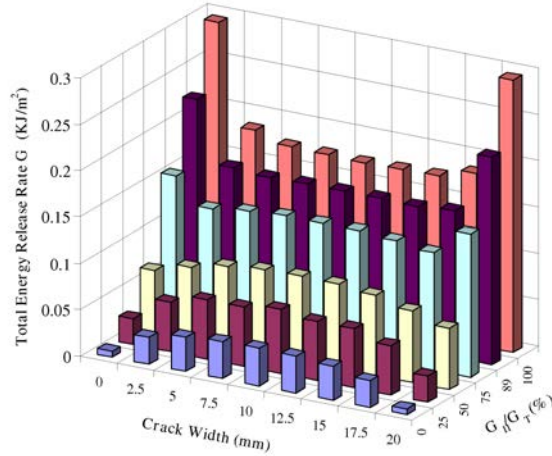$G_{II}/G_T = 0.5$.

FIG. 18. Distribution of G_T in the crack width with VCCT.

11. CONCLUSION

2D model and plane strain conditions can not explain completely the stress distribution in crack width and regarding the above behaviors, the fracture toughness of the 3D model is lower than the 2D model. 3D effects of model are applied as a percentage of error to the results of fracture toughness of 2D model. The curve of the fracture toughness for a crack length of 35mm, in the tested mixed modes, versus numerical results of 2D and 3D, and also experimental results of 5%, NL and AE criteria, are drawn in Fig. 19. Experimental
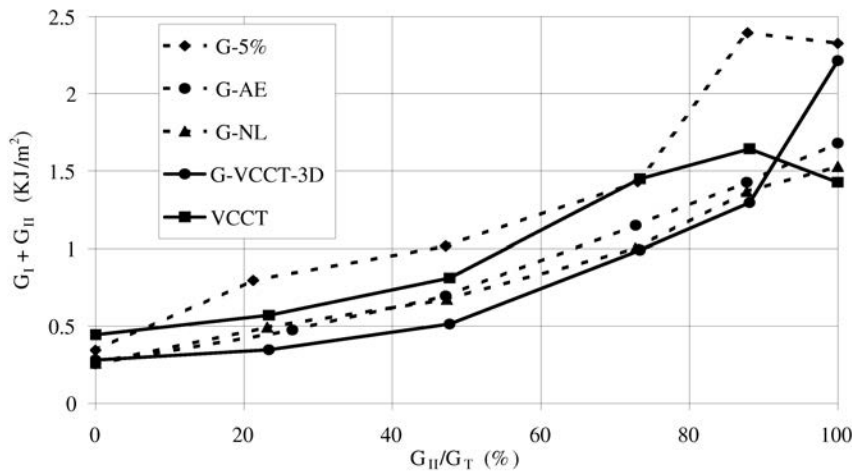

FIG. 19. Fracture toughness using experimental criterions and numerical analysis for different modes of loading.

results of NL and AE have a better agreement with each other, for the ratios of G_{II}/G_T, from 0 to 89%. The fracture toughness of 3D model G_{3D} has decreased in maximum by 39% relative to the fracture toughness of 2D model G_{2D}, and for the pure Mode II loading has increased by 35%. In all the cases with increasing of Mode II loading component, the fracture toughness increases.

Although this finite element code doesn't contain a complete model of the fracture mechanisms at the crack tip, however with taking into account the 3D effect, the numerical results are brought to the vicinity of the experimental results. The effects like friction between the two faces of the crack, kind of the specimen supports and so on, which need statistical studies, should also enter in the mechanisms of the fracture and their influence on the SERR rate should be studied.

References

1. R.M. JONES, *Mechanics of composite materials*, 2-nd edition, Taylor and Francis, Inc. USA, 1999.

2. N.E. JANSON, R. LARSON, *Rotational interface formulation for delamination analysis of composite laminates*, Computers and Structures, **81**, 2705–2716, 2003.

3. R. KRUEGER, M. CVITKOVICH, K. O'BRIEN, P. MINGUET, *Testing and analysis of composite skin/stringer*, J. Composite Materials, **34**, 15, 1263–1300, 2000.

4. M.R. KHOSHRAVAN, A.R. JAMI, *Interlaminar stresses in CFRP composites*, Proceeding of the International Conference on Advanced Fibers and Polymer Materials, Oct. 19–21, Shanghai, China, **1**, 338–342, 2005.

5. R. HERTZBERG, *Deformation and fracture mechanics of engineering materials*, Section 8.2, Wiley publishing company, 1989.

6. M.R. KHOSHRAVAN, M. MONIR VAGHEFI, *Numerical evaluation of delamination on Mode II in glass fiber reinforced composites*, Engineering Transactions, **53**, 55–68, 2005.

7. F. DUCEPT, P. DAVIES, D. GAMBY, *An experimental study to validate tests used to determine mixed mode failure criteria of glass/epoxy composite*, Composite Part A 28A, 719–729, 1997.

8. Z. ZOU, S.R. REID, S. LI, *A continuum damage model for delaminations in laminated composites*, J. Mechanics and Physics of Solids, **51**, 333–356, 2003.

9. J.H. CREWS, J.R. REEDER, *A mixed mode bending apparatus for delamination testing*, NASA TECHNICAL MEMORANDUM 100662, 1988.

10. J.R. REEDER AND J.H. CREWS, *Nonlinear analysis and redesign of the mixed mode bending delamination test*, NASA TECHNICAL MEMORANDUM 102777, 1991.

11. F. DUCEPT, P. DAVIES, D. GAMBY, *Mixed mode failure criteria for a glass/epoxy composite and an adhesively bonded composite/composite joint*, International Journal of Adhesion and Adhesives, **20**, 233–244, 2000.

12. G.R. IRWIN, *Fracture Handbook of Physic, VI*, Springer, 551–590, 1958.

13. M.F. KANNINEN, *An argumented double cantilever beam model for studying crack propagation and arrest*, International Journal of Fracture, **9**, 1, 83–92,1973.

14. S. HASHEMI, A.J. KINLOCH, J.G. WILLIAMS, *The analysis of interlaminar fracture in uniaxial fiber-polymer composites*, Proceedings of the Royal Society of London, A427,173–199,1990.

15. R. KRUEGER, T.K. O'BRIEN, *A shell/3D modeling technique for the analysis of delaminated composite laminates*, J. of Composites, Part A: Applied Science and Manufacturing, **32**, 1, 25–44,2001.

16. P. DAVIES, *Analysis of G_{IC} interlaminar fracture test*, Applied Composite Materials, Round robin, 1996.

17. ASTM standard E399-81, *Standard test method for plane strain fracture toughness of metallic materials.*